Pergamon

Int. J. Solids Structures Vol. 32, No. 14, pp. 2077–2093, 1995
Elsevier Science Ltd
Printed in Great Britain

0020–7683(94)00197–9

STRESSES IN A SPHERICAL PRESSURE VESSEL UNDERGOING CREEP AND DIMENSIONAL CHANGES†

G. K. MILLER
Idaho National Engineering Laboratory, EG&G Idaho, Inc., Idaho Falls, ID 83415, U.S.A.

(*Received* 12 *November* 1993; *in revised form* 9 *August* 1994)

Abstract—A solution is presented for stresses and displacements in a thick spherical shell subjected to internal and external pressure loads. In addition to elastic behavior, the shell material is assumed to undergo both creep and dimensional changes as the shell is pressurized. The dimensional changes considered are (1) anisotropic swelling or shrinkage induced by neutron irradiation of the shell, or (2) isotropic thermal expansion with a temperature gradient through the shell wall. This solution was developed for pressure vessel modeling of fuel and target particles of the New Production Modular High Temperature Gas-Cooled Reactor (NP–MHTGR), where it is used in predicting particle failure probabilities for large particle batches. It has the advantage that it is computationally much faster than finite element or finite difference approaches. The creep behavior is initially represented with a 4-parameter linear viscoelastic model to include transient and steady-state components, then is extended to more general linear viscoelastic models. The analytical approach, which is applied to a spherical geometry here, may be useful in solving for similar loadings on other vessel geometries.

NOTATION

ε strain
t time, (sec), or neutron fluence, (n/m^2)
E modulus of elasticity, (MPa)
c creep coefficient, (MPa–sec)$^{-1}$ or (MPa–n/m^2)$^{-1}$
σ stress, (MPa)
μ Poisson's ratio
ν Poisson's ratio in steady-state creep
γ Poisson's ratio in transient creep
S strain rate due to dimensional changes, (sec)$^{-1}$
u radial displacement, (m)
r radial coordinate, (m)
p internal pressure, (MPa)
q external pressure, (MPa)
α coefficient of thermal expansion, (m/m-°K)
T rate of change in temperature, (°K/sec)

Subscripts:
r radial
t tangential (hoop)

1. INTRODUCTION

This development concerns time-dependent stresses and displacements in a thick spherical shell that undergoes creep and dimensional change behavior in addition to elastic response during the time it is pressurized. The dimensional changes considered are (1) anisotropic swelling or shrinkage induced by neutron irradiation of the shell, or (2) isotropic thermal expansion with a temperature gradient through the shell wall. This solution was developed for pressure vessel modeling of fuel and target particles of the New Production Modular High Temperature Gas-Cooled Reactor (NP–MHTGR). The prototypical nuclear fuel of the NP–MHTGR consists of spherical TRISO-coated particles suspended in graphite cylinders, which are placed in hexagonal graphite blocks. The three coating layers (IPyC, SiC, and OPyC) act as a pressure vessel for fission product gases as well as a barrier to the migration of other fission products. These particles also contain a buffer

† Work supported by the U.S. Department of Energy under DOE Idaho Operations Office Contract DE–AC07–76ID01570.

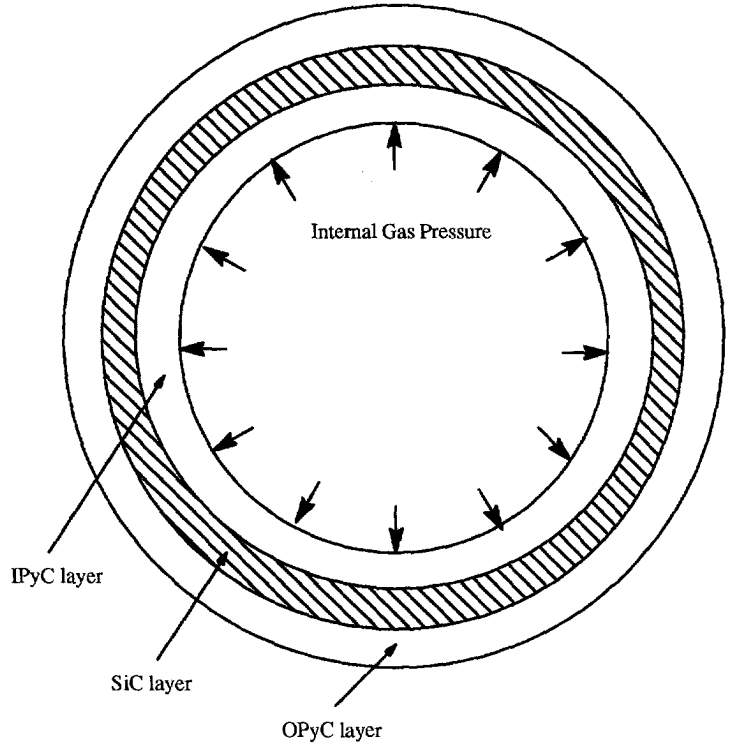

Fig. 1. Three-layer spherical shell geometry.

between the kernel and the three outer layers. Since the buffer is a porous medium, though, it makes no structural contribution to the pressure vessel. The target particles are similarly TRISO-coated particles, but of a larger size. The coating layers of the targets act like a pressure vessel for fission product gases, but also serve to retain tritium. The geometry for the three outer layers of the fuel or target particles is shown in Fig. 1. Multilayered spherical fuel particles are also used to fuel other reactors, such as particle-bed reactors that power space vehicles (Dobranich and El-Genk, 1991).

Of concern is what portion of a particle population can be expected to fail under conditions experienced in the NP–MHTGR. Because of statistical variations in particle dimensions, fuel enrichment, material strengths, etc., each particle in a batch is unique. Addressing the concern about particle failures requires that models of the mechanical behavior of the coating layers be developed to predict stresses in this pressure vessel and thereby determine particle batch failure probabilities. The behavior of the pyrocarbon layers (IPyC and OPyC) is complicated by the fact that they exhibit irradiation-induced creep and anisotropic swelling behavior under fast neutron irradiation (Kaae, 1975). The pyrocarbons also seem to exhibit thermal-induced creep at elevated temperatures, which could occur during accident conditions. The SiC layer is considered to remain an elastic medium under the conditions considered (Price, 1977). Because of their brittle nature, the pyrocarbon and SiC layers incur essentially no plastic deformations at any stress level. At the outset, there are three alternatives for determining behavior of the spherical layers in the particles, namely (1) finite element analysis, (2) finite difference analysis, or (3) an analytical solution. An analytical solution has at least two advantages over finite element or finite difference approaches:

(1) The solution, when programmed for computer calculation, is computationally much faster. The solution can greatly reduce computational time when batch failure probabilities are calculated using the Monte Carlo method.
(2) An analytical solution lends greater insight into the problem.

A closed-form analytical solution was previously developed for stresses at the interfaces in a three-layer particle experiencing the irradiation-induced behavior described above (Miller and Bennett, 1993). The solution incorporated the assumption that, in irradiation-induced creep, the PyC layers exhibit steady-state creep behavior, i.e. the creep strain rates are proportional to the level of stress in the pyrocarbons. Some material property data for the pyrocarbons used in the particles of the NP-MHTGR raise the possibility, though, that a complete model of the pyrocarbon behavior may require the addition of a transient creep component. In addition to including transient creep response, a fuller description of particle behavior is attained if stresses and displacements are determined throughout the thickness of a spherical layer.

Thus, the method used in the solution above is employed here to develop general time-dependent expressions for radial and tangential stresses and displacement throughout a pressurized sphere that undergoes creep and swelling. The creep model, which previously included just steady-state creep, is expanded to include transient creep. The creep behavior is represented initially with a 4-parameter linear viscoelastic model. It is then shown how other more general linear viscoelastic models can be incorporated. The method is then used to solve the case where dimensional changes in the sphere are isotropic but have a gradient through the thickness, representative of behavior at elevated temperatures. In practice, a creep law has not yet been developed for thermal creep in the pyrocarbons. In the solution for elevated temperatures, the creep behavior is again modeled with linear viscoelastic models.

The accuracy of solutions for the single-layer sphere are verified by making comparisons with results obtained from finite element viscoelastic analyses, and by assuring that the solutions reduce appropriately to established solutions when creep strains are disregarded. A solution for three-layer particles can be obtained by imposing displacement continuity at the interfaces. Though a complete solution for a three-layer particle is not presented, the single-layer solution is used here to investigate behavior of a two-layer particle having a rigid interface.

2. THEORY AND DERIVATION

The stresses analyzed herein are those resulting from creep and dimensional changes of a thick spherical shell together with uniform internal and external pressures applied to the surfaces of the shell. The strain rates due to swelling are assumed to vary with time, while the creep coefficients are assumed to be constant. Other material properties, such as Young's elastic moduli and Poisson's ratios, are also assumed to be constant. In the solution, the Poisson's ratios in creep are set equal to 0.5, meaning that there is no volumetric change due to creep. This assumption of incompressibility, which is normally used in plasticity theory, simplifies the derivations. The solution technique could, however, accomodate other values for these Poisson's ratios.

The creep behavior is modeled with a 4-parameter Voigt model (Tschoegl, 1989), shown in Fig. 2. This model consists of a Maxwell element in series with a Kelvin element. The Maxwell element consists of an elastic element represented by a linear spring in series with a viscous fluid element represented by a dashpot. This element models instantaneous elastic response and steady-state creep deformation. The Kelvin element consists of a linear spring in parallel with a dashpot. This element models the strain retardation behavior of transient creep. The total strain for the 4-parameter Voigt model is

$$\varepsilon = \varepsilon_1 + \varepsilon_2 + \varepsilon_3 \tag{1}$$

where ε_1 and ε_3 are the strains in the spring and dashpot of the Maxwell element, respectively, and ε_2 is the strain in the Kelvin element. Each of these three elements experiences the same stress. The constitutive equation for each is as follows:

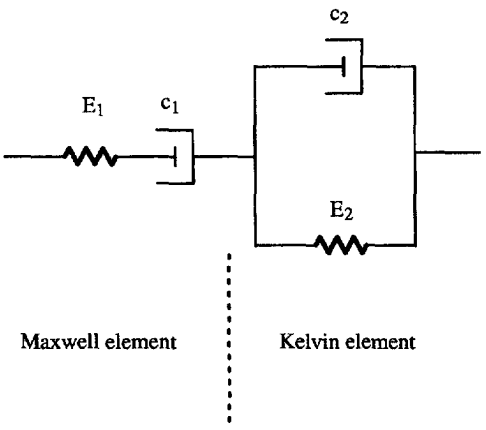

Fig. 2. 4-parameter Voigt model.

$$\sigma = E_1 \varepsilon_1 \tag{2}$$

$$\sigma = E_2\left(\varepsilon_2 + \frac{\dot{\varepsilon}_2}{E_2 c_2}\right) \tag{3}$$

$$\sigma = \frac{\dot{\varepsilon}_3}{c_1} \tag{4}$$

where the dots indicate differentiation with respect to time. Solving for ε_2 in eqn (3) gives

$$\varepsilon_2 = c_2 e^{-E_2 c_2 t} \int_0^t e^{E_2 c_2 t'} \sigma \, \mathrm{d}t'. \tag{5}$$

Thus, the total strain rate for a 4-parameter Voigt creep model becomes

$$\frac{\partial \varepsilon}{\partial t} = \frac{1}{E_1}\frac{\partial \sigma}{\partial t} + (c_1 + c_2)\sigma - E_2 c_2^2 e^{-E_2 c_2 t} \int_0^t e^{E_2 c_2 t'} \sigma \, \mathrm{d}t'. \tag{6}$$

This model differs from that used previously with the inclusion of the transient creep response. When Poisson effects are considered in the spherical geometry of the shell, and strain rates due to dimensional changes are included, the constitutive equations for the radial and tangential directions become

$$\frac{\partial \varepsilon_r}{\partial t} = \frac{1}{E_1}\left(\frac{\partial \sigma_r}{\partial t} - 2\mu \frac{\partial \sigma_t}{\partial t}\right) + (c_1 + c_2)(\sigma_r - 2\gamma\sigma_t) - E_2 c_2^2 e^{-E_2 c_2 t} \int_0^t e^{E_2 c_2 t'} (\sigma_r - 2\gamma\sigma_t) \, \mathrm{d}t' + S_r \tag{7}$$

$$\frac{\partial \varepsilon_t}{\partial t} = \frac{1}{E_1}\left[(1-\mu)\frac{\partial \sigma_t}{\partial t} - \mu \frac{\partial \sigma_r}{\partial t}\right] + (c_1 + c_2)[(1-\gamma)\sigma_t - \gamma\sigma_r]$$

$$- E_2 c_2^2 e^{-E_2 c_2 t} \int_0^t e^{E_2 c_2 t'} [(1-\gamma)\sigma_t - \gamma\sigma_r] \, \mathrm{d}t' + S_t. \tag{8}$$

The dimensional changes are shown to be anisotropic, denoted by strain rates S_r and S_t. The variable t can represent either neutron fluence or time in the solution.

Equations (7) and (8) are accompanied by the strain–displacement and equilibrium relations for a spherical system (Sokolnikoff, 1956):

$$\varepsilon_r = \frac{\partial u}{\partial r} \tag{9}$$

$$\varepsilon_t = \frac{u}{r} \tag{10}$$

$$\frac{\partial \sigma_r}{\partial r} + \frac{2}{r}(\sigma_r - \sigma_t) = 0. \tag{11}$$

2.1. *Irradiation-induced creep and swelling*

In irradiation-induced creep and swelling, the strain rates due to swelling have time dependence but not spatial dependence. As was done previously, it is advantageous to assume a solution of eqns (7) through (11) of the following general form:

$$u(r, t) = \sum_{i=0}^{\infty} u_i(r) t^i \tag{12}$$

$$\sigma_r(r, t) = \sum_{i=0}^{\infty} \sigma_{ri}(r) t^i \tag{13}$$

$$\sigma_t(r, t) = \sum_{i=0}^{\infty} \sigma_{ti}(r) t^i \tag{14}$$

and to expand the strain rates S_r and S_t into series having components $S_{ri}t_i$ and $S_{ti}t_i$. Utilizing this solution in eqns (7) through (11), and setting $\nu = \gamma = 0.5$, it is found that a general differential equation for the u_i becomes ($i \geqslant 0$)

$$\frac{d^2 u_i}{dr^2} + \frac{2}{r}\frac{du_i}{dr} - \frac{2}{r^2} u_i = 2\frac{(k-m)}{r} f_i \tag{15}$$

where

$$k = \frac{1-\mu}{E_1} \quad m = \frac{\mu}{E_1} \tag{16}$$

and the f_i can be generated from

$$f_{i+1} = -\frac{(c_1+c_2)}{2k}\frac{f_i}{i+1} + \frac{S_{ri}-S_{ti}}{k(i+1)} - \frac{c_2}{2k(i+1)} \sum_{n=1}^{i} f_{i-n}(-E_2 c_2)^n \frac{(i-n)!}{i!}, \quad f_0 = 0. \tag{17}$$

The solutions for u_i, σ_{ri}, and σ_{ti} become

$$u_i = A_i r + B_i r^{-2} + \frac{2(k-m)}{3} f_i r \ln r \tag{18}$$

$$\sigma_{ri} = \frac{A_i}{k-m} - \frac{2B_i r^{-3}}{l+m} + 2f_i \frac{[(l+m)\ln r + k]}{3(l+m)} + \frac{(c_1+c_2)}{i(l+m)}(\sigma_{t,i-1} - \sigma_{r,i-1}) + \frac{c_2}{i(l+m)} \sum_{n=1}^{i-1} (\sigma_{t,i-n-1} - \sigma_{r,i-n-1})(-E_2 c_2)^n \frac{(i-n)!}{i!} - \frac{kS_{r,i-1} + hS_{t,i-1}}{i(kl-hm)} \tag{19}$$

$$\sigma_{ti}-\sigma_{ri}=\frac{3B_i r^{-3}}{l+m}-\frac{2f_i(k-m)}{3(l+m)}-\frac{3(c_1+c_2)}{2i(l+m)}(\sigma_{t,i-1}-\sigma_{r,i-1})$$
$$-\frac{3c_2}{2i(l+m)}\sum_{n=1}^{i-1}(\sigma_{t,i-n-1}-\sigma_{r,i-n-1})(-E_2c_2)^n\frac{(i-n)!}{i!}+\frac{S_{r,i-1}-S_{t,i-1}}{i(l+m)} \quad (20)$$

where

$$l=\frac{1}{E_1}\quad h=\frac{2\mu}{E_1}. \quad (21)$$

In these equations, quantities having a negative index are to be neglected.

The internal and external pressures, $p(t)$ and $q(t)$, are applied at the inner and outer radii, respectively, by expressing them in the form

$$p(t)=\sum_{i=0}^{\infty}p_i t^i \qquad q(t)=\sum_{i=0}^{\infty}q_i t^i. \quad (22)$$

The pressures p and q will be treated as positive outward.

Using eqn (19) to equate the radial stress to these pressures at the surfaces results in the following useful expressions:

$$A_i=\frac{k-m}{(r_2^{-3}-r_1^{-3})}\left[p_i r_2^{-3}-q_i r_1^{-3}+\frac{2}{3}f_i(r_1^{-3}\ln r_2-r_2^{-3}\ln r_1)\right]+\frac{S_{r,i-1}+2S_{t,i-1}}{3i} \quad (23)$$

$$B_i=\frac{(l+m)}{2(r_2^{-3}-r_1^{-3})}\left\{p_i-q_i-\frac{2}{3}f_i\ln\frac{r_1}{r_2}-\frac{c_1+c_2}{i(l+m)}\left[-\frac{3}{2}(p_{i-1}-q_{i-1})+f_{i-1}\ln\frac{r_1}{r_2}\right]\right\}$$
$$-\frac{c_2}{2i(r_2^{-3}-r_1^{-3})}\sum_{n=1}^{i-1}\left[-\frac{3}{2}(p_{i-n-1}-q_{i-n-1})+f_{i-n-1}\ln\frac{r_1}{r_2}\right](-E_2c_2)^n\frac{(i-n)!}{i!} \quad (24)$$

$$\sigma_{ti}-\sigma_{ri}=\frac{3r^{-3}}{2(r_2^{-3}-r_1^{-3})}\left[p_i-q_i-\frac{2}{3}f_i\ln\frac{r_1}{r_2}\right]+\frac{f_i}{3}. \quad (25)$$

Substituting eqns (23) through (25) into eqn (19), substituting the result into eqn (13), and summing all terms in the series gives the following general expression for radial stress in the shell:

$$\sigma_r(r,t)=\frac{r_1^3(r_2^3-r^3)}{r^3(r_2^3-r_1^3)}p-\frac{r_2^3(r_1^3-r^3)}{r^3(r_2^3-r_1^3)}q-\frac{2}{3}\left[\frac{r_1^3(r_2^3-r^3)\ln r_1-r_2^3(r_1^3-r^3)\ln r_2}{r^3(r_2^3-r_1^3)}-\ln r\right]F(t). \quad (26)$$

The last term in eqn (26) vanishes at the boundaries. Here

$$F(t)=\sum_{i=0}^{\infty}f_i t^i. \quad (27)$$

Using eqn (17),

$$F=\sum_{i=1}^{\infty}\left[-\frac{(c_1+c_2)}{2ki}f_{i-1}+\frac{S_{r,i-1}-S_{t,i-1}}{ki}\right]t^i-\frac{c_2}{2k}\sum_{i=1}^{\infty}\frac{1}{i}\left(\sum_{n=1}^{i-1}f_{i-n-1}(-E_2c_2)^n\frac{(i-n)!}{i!}\right)t^i. \tag{28}$$

Differentiating with respect to t, eqn (28) becomes the following differential equation:

$$\frac{dF}{dt}+\frac{1}{2k}\left[(c_1+c_2)F-E_2c_2^2e^{-E_2c_2t}\int_0^t e^{E_2c_2t'}F\,dt'\right]=\frac{S_r-S_t}{k}. \tag{29}$$

This equation is subject to the initial condition that F equals zero, since $f_0=0$. It can be readily solved by numerical analysis. It is solvable in closed form if there is no transient creep, provided that the swelling rate histories are represented by closed form functions. A swelling rate history can typically be curve fit with a polynomial to whatever order is needed.

Equations (18) and (23) through (25) can then be used to develop the following general expressions for the tangential stress and radial displacement:

$$\sigma_t(r,t)=-\frac{r_1^3(2r^3+r_2^3)}{2r^3(r_2^3-r_1^3)}p+\frac{r_2^3(2r^3+r_1^3)}{2r^3(r_2^3-r_1^3)}q+\frac{1}{3}\left[\frac{r_1^3(r_2^3+2r^3)\ln r_1-r_2^3(r_1^3+2r^3)\ln r_2}{r^3(r_2^3-r_1^3)}+2\ln r+1\right]F \tag{30}$$

$$\begin{aligned}u(r,t)=&-\frac{2r^3r_1^3(k-m)+r_1^3r_2^3(l+m)}{2r^2(r_2^3-r_1^3)}p+\frac{2r^3r_2^3(k-m)+r_1^3r_2^3(l+m)}{2r^2(r_2^3-r_1^3)}q\\&-\frac{3r_1^3r_2^3}{4r^2(r_2^3-r_1^3)}\int_0^t\left[(p-q)(c_1+c_2)-E_2c_2^2e^{-E_2c_2t'}\int_0^{t'}e^{E_2c_2t''}(p-q)\,dt''\right]dt'\\&+\frac{r_1^3r_2^3(\ln r_1-\ln r_2)}{r^2(r_2^3-r_1^3)}\int_0^t(S_r-S_t)\,dt'+\frac{r}{3}\int_0^t(S_r+2S_t)\,dt'\\&-\frac{2}{3}(k-m)\left[\frac{r^3(r_2^3\ln r_2-r_1^3\ln r_1)+r_1^3r_2^3(\ln r_1-\ln r_2)}{r^2(r_2^3-r_1^3)}-r\ln r\right]F.\end{aligned} \tag{31}$$

The last term in eqn (31) vanishes at the boundaries. When there is no creep or swelling, eqns (26), (30) and (31) reduce to the solution for a pressurized elastic spherical shell (Lin, 1968).

2.2. *Other linear viscoelastic models*

In the development above, the elastic and creep behavior were modeled with the 4-parameter Voigt element shown in Fig. 2. The solution can be extended to include other linear viscoelastic models. Representing the creep strain rate by an operator P acting on the stress σ, eqn (6) can be rewritten in the form

$$\frac{\partial\varepsilon}{\partial t}=\frac{1}{E_1}\frac{\partial\sigma}{\partial t}+P(\sigma). \tag{32}$$

In the development of eqn (17), which leads to eqn (29), it can be shown that if the creep strain rate operator (P) acts linearly on the stress, such that

$$P(\sigma_r - \sigma_t) = P(\sigma_r) - P(\sigma_t) \tag{33}$$

then eqn (29) can be written as

$$\frac{dF}{dt} + \frac{1}{2k} P(F) = \frac{S_r - S_t}{k}. \tag{34}$$

This would be the case for linear viscoelastic models where the strain rate can be written in terms of stress, such as a generalized Voigt model. The generalized Voigt model contains many Kelvin elements in series (Tschoegl, 1989). The expressions for stresses and displacements, eqns (26), (30), and (31), are unchanged except that the third term of eqn (31) becomes

$$-\frac{3r_1^3 r_2^3}{4r^2(r_2^3 - r_1^3)} \int_0^t P(p-q)\, dt'. \tag{35}$$

Cases where the operator P acts nonlinearly on the stress would have to be treated individually, and could require that approximations be applied.

2.3. *Boundary conditions*

When boundary conditions are known in the form of pressure histories at the surfaces of the shell, these can be readily substituted into eqns (26), (30), and (31) to determine stresses and displacements throughout the shell. If a displacement boundary condition is specified, then eqn (31) must be used to determine any unknown pressure histories before eqns (26) and (30) can be used to determine stresses. For example, if a displacement history is specified for the inner surface and there is no external pressure applied, then eqn (31) applied at r_1 becomes

$$a\frac{dp}{dt} + b\left[p(c_1 + c_2) - E_2 c_2^2 e^{-E_2 c_2 t} \int_0^t e^{E_2 c_2 t'} p\, dt'\right] = g(t) + \frac{du}{dt}(r_1, t) \tag{36}$$

where a and b are constants and $g(t)$ is a function dependent on the swelling rate histories. This equation is of the same form as eqn (29) and, therefore, can be solved using the same numerical procedure.

2.4. *Isotropic thermal expansion with a gradient through the shell thickness*

In accident conditions, the coated particles could be exposed to elevated temperatures (to 1500°C or higher). At elevated temperatures, tritium retained by target particles permeates through the particle layers at a rate dependent on the temperature. A particle that fails during this time gives an instantaneous burst of tritium release. The ability to determine particle failures caused by high temperatures aids in predicting the quantity of tritium released through an elevated temperature period. The higher temperatures increase the particle internal gas pressure. Results from tests on NP-MHTGR target particles also indicate that thermal expansion in the particles is accompanied by thermal creep in the pyrocarbon layers. The attendant stress relaxation in these layers increases the stress in the SiC layer, contributing to particle failures. Therefore, the methods used above are applied here to the problem where the dimensional changes (expansion) have a gradient through the wall thickness. For simplicity, the thermal expansion is assumed to be isotropic, though the solution technique would permit anisotropic expansion. The creep in this case is temperature-induced rather than irradiation-induced. A thermal creep law has not yet been established for the pyrocarbons, so it is not certain that a linear viscoelastic creep model is appropriate for thermal creep behavior in these layers. The thermal creep behavior of some materials, such as polymers, is well represented with linear viscoelastic models (Ferry, 1980). In metals, however, the relation between creep strain rate and stress is generally

nonlinear (Lin, 1968). For most metals, this relation is approximately linear for a range of stress and temperature, and a linear viscoelastic model can be applied over this range. Similarly, a linear viscoelastic model is likely to be representative of thermal creep behavior of the pyrocarbons for at least a range of stress and temperature. The thermal creep and elastic behavior, then, will be represented with a 4-parameter Voigt model. As before, this representation can be extended to other linear viscoelastic models.

The strain rates represented by S_r and S_t in eqns (7) and (8) will both be set equal to αT. In thermal expansion, α is the expansion coefficient and T is the rate of change in temperature. T will be expressed in the following form:

$$T(r,t) = \sum_{i=0}^{\infty} \sum_{j=0}^{\infty} a_{ij} r^j t^i. \tag{37}$$

This distribution is symmetrical with respect to the center of the sphere, but does have a radial dependence. Using the solution form of eqns (12) through (14) in eqns (7) through (11), it is found that the general differential equation for the u_i becomes ($i \geqslant 0$)

$$\frac{d^2 u_i}{dr^2} + \frac{2}{r}\frac{du_i}{dr} - \frac{2}{r^2} u_i = \sum_{j=1}^{\infty} j r^{j-1} \left[2(k-m) g_{ij} + \frac{3\alpha}{i} a_{i-1,j} \right] \tag{38}$$

where any term with a negative index is to be neglected. The g_{ij} can be generated from

$$g_{i+1,j} = -\frac{(c_1+c_2)}{2k}\frac{g_{ij}}{i+1} - \frac{\alpha}{k(i+1)} a_{ij} - \frac{c_2}{2k(i+1)} \sum_{n=1}^{i} g_{i-n,j} (-E_2 c_2)^n \frac{(i-n)!}{i!}, \quad g_{0j} = 0 \tag{39}$$

In this case, the general solutions for u_i, σ_{ri}, and σ_{ti} become

$$u_i = A_i r + B_i r^{-2} + \sum_{j=1}^{\infty} \frac{r^{i+1}}{j+3} \left[2(k-m) g_{ij} + \frac{3\alpha}{i} a_{i-1,j} \right] \tag{40}$$

$$\begin{aligned} \sigma_{ri} = {} & \frac{A_i}{k-m} - \frac{2B_i r^{-3}}{l+m} + \frac{(c_1+c_2)}{i(l+m)} (\sigma_{t,i-1} - \sigma_{r,i-1}) \\ & + \frac{c_2}{i(l+m)} \sum_{n=1}^{i-1} (\sigma_{t_{i-n-1}} - \sigma_{r_{i-n-1}}) (-E_2 c_2)^n \frac{(i-n)!}{i!} \\ & + \sum_{j=1}^{\infty} \left\{ g_{ij} r^j \left[\frac{2k(j+1)+4m}{(l+m)(j+3)} \right] + a_{i-1,j} r^i \left[\frac{2\alpha j}{i(l+m)(j+3)} \right] \right\} \end{aligned} \tag{41}$$

$$\begin{aligned} \sigma_{ti} - \sigma_{ri} = {} & \frac{3B_i r^{-3}}{l+m} - \frac{3(c_1+c_2)}{2i(l+m)} (\sigma_{t,i-1} - \sigma_{r,i-1}) \\ & - \frac{3c_2}{2i(l+m)} \sum_{n=1}^{i-1} (\sigma_{t,i-n-1} - \sigma_{r,i-n-1}) (-E_2 c_2)^n \frac{(i-n)!}{i!} \\ & - \sum_{j=1}^{\infty} \left[g_{ij} r^j \frac{2j(k-m)}{(l+m)(j+3)} + a_{i-1,j} r^j \frac{3\alpha j}{i(l+m)(j+3)} \right] \end{aligned} \tag{42}$$

Applying pressure conditions at the boundaries results in expressions similar to eqns (23) and (24) for A_i and B_i, and the following for $\sigma_{ti} - \sigma_{ri}$:

$$\sigma_{ti}-\sigma_{ri}=\frac{3r^{-3}}{2(r_2^{-3}-r_1^{-3})}\left[p_i-q_i+\sum_{j=1}^{\infty}\frac{2g_{ij}(r_2^j-r_1^j)}{j+3}\right]+\sum_{j=1}^{\infty}\frac{g_{ij}r^j j^i}{j+3}. \tag{43}$$

It is advantageous to define a function $G(r,t)$ as follows:

$$G(r,t)=\sum_{i=0}^{\infty}\sum_{j=0}^{\infty}g_{ij}r^j t^i. \tag{44}$$

Using eqn (39), it can be shown that $G(r,t)$ satisfies the following differential equation:

$$\frac{\partial G}{\partial t}+\frac{1}{2k}\left[(c_1+c_2)G-E_2c_2^2e^{-E_2c_2t}\int_0^t e^{E_2c_2t'}G\,\mathrm{d}t'\right]=-\frac{\alpha}{k}T \tag{45}$$

with the initial condition that G equal zero. For other viscoelastic models, where the creep strain rate can be represented by an operator P that acts linearly on the stress (see Section 2.2), this equation would become

$$\frac{\partial G}{\partial t}+\frac{1}{2k}P(G)=-\frac{\alpha}{k}T. \tag{46}$$

The expressions for A_i, B_i, and $\sigma_{ti}-\sigma_{ri}$ can then be used in eqns (40) through (42) to develop the following general equations for stresses and displacement:

$$\sigma_r(r,t)=\frac{r_1^3(r_2^3-r^3)}{r^3(r_2^3-r_1^3)}p-\frac{r_2^3(r_1^3-r^3)}{r^3(r_2^3-r_1^3)}q+\frac{2}{r^3(r_2^3-r_1^3)}\left[(r_2^3-r^3)\int_{r_1}^{r}r'^2G\,\mathrm{d}r'-(r-r_1^3)\int_r^{r_2}r'^2G\,\mathrm{d}r'\right] \tag{47}$$

$$\sigma_t(r,t)=-\frac{r_1^3(2r^3+r_2^3)}{2r^3(r_2^3-r_1^3)}p+\frac{r_2^3(2r^3+r_1^3)}{2r^3(r_2^3-r_1^3)}q+G-\frac{2r^3+r_2^3}{r^3(r_2^3-r_1^3)}\int_{r_1}^{r}r'^2G\,\mathrm{d}r'-\frac{2r^3+r_1^3}{r^3(r_2^3-r_1^3)}\int_r^{r_2}r'^2G\,\mathrm{d}r' \tag{48}$$

$$\begin{aligned}u(r,t)=&-\frac{2r^3r_1^3(k-m)+r_1^3r_2^3(l+m)}{2r^2(r_2^3-r_1^3)}p+\frac{2r^3r_2^3(k-m)+r_1^3r_2^3(l+m)}{2r^2(r_2^3-r_1^3)}q\\&-\frac{3r_1^3r_2^3}{4r^2(r_2^3-r_1^3)}\int_0^t\left[(p-q)(c_1+c_2)-E_2c_2^2e^{-E_2c_2t'}\int_0^{t'}e^{E_2c_2t''}(p-q)\,\mathrm{d}t''\right]\mathrm{d}t'\\&+\frac{3\alpha}{r^2(r_2^3-r_1^3)}\int_0^t\left(r_2^3\int_{r_1}^{r}r'^2T\,\mathrm{d}r'+r_1^3\int_r^{r_2}r'^2T\,\mathrm{d}r'\right)\mathrm{d}t'\\&-\frac{2(k-m)}{r^2(r_2^3-r_1^3)}\left[(r^3-r_2^3)\int_{r_1}^{r}r'^2G\,\mathrm{d}r'+(r^3-r_1^3)\int_r^{r_2}r'^2G\,\mathrm{d}r'\right].\end{aligned} \tag{49}$$

Again, the third term of eqn (49) is modified per eqn (35) for other viscoelastic models. When there is no creep,

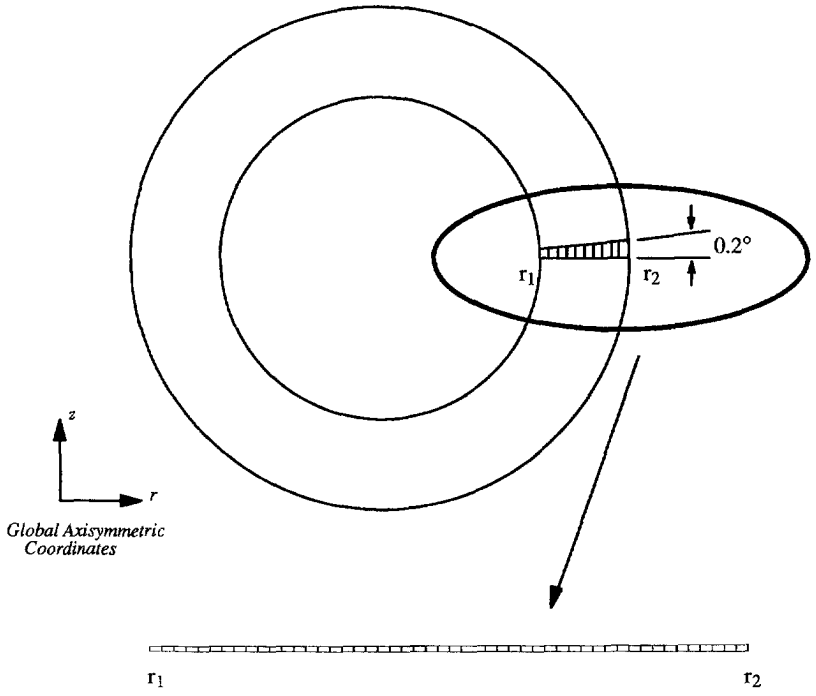

Fig. 3. ABAQUS model using axisymmetric finite elements.

$$\frac{\partial G}{\partial t} = -\frac{a}{k}T \tag{50}$$

and eqns (47) through (49) reduce to the solution for thermal stresses in an elastic spherical shell (Timoshenko and Goodier, 1951).

3. COMPARISON WITH FINITE ELEMENT VISCOELASTIC ANALYSIS

The equations developed above for the case of irradiation-induced creep and swelling [eqns (26), (30), and (31)] were tested by making a comparison with results obtained from a viscoelastic analysis using the ABAQUS computer program (1992). The ABAQUS model of Bennett (1991) was used to perform these analyses. The model, in this case, consists of a row of 50 axisymmetric elements representing a single layered spherical shell, as shown in Fig. 3. The elements are arranged in the radial direction, comprising a thin spherical sector. Application of appropriate boundary conditions gave the model spherical symmetry.

The problem selected for comparison involves a spherical shell having the dimensions, applied pressures, creep coefficients, and dimensional change rates listed in Table 1. The creep model was input to the ABAQUS program with a user subroutine. The integral in the creep law of eqn (6) was compiled through the solution with the use of "state variables." Comparisons were made at times of 0.4×10^7 and 1.2×10^7 sec into the solution. The function $F(t)$ was obtained by a numerical solution to eqn (29). Results of the comparisons are shown in Figs 4 and 5, where plots of the radial and tangential stresses through the shell thickness are presented. There is no discernable difference between the solutions.

The displacement equation (31), was tested by imposing a rigid boundary condition ($u = 0$) at the inner radius of the sphere. All other conditions were identical to the problem solved above. The pressure $p(t)$ at the inner radius was solved for using eqn (31) in the manner described in Section 2.3. During this numerical solution, the radial and tangential stresses through the thickness were solved for using eqns (26) and (30). Comparisons with an ABAQUS solution at a time of 1.2×10^7 sec for this problem are presented in Fig. 6, where again an excellent correlation was attained.

Table 1. Parameters used in test problem

Parameter	Value	Units
r_1	200	μm
r_2	250	μm
E_1	3×10^4	MPa
E_2	4×10^4	MPa
μ	0.33	
S_{r0}	-1×10^{-8}	$\sec^{-1}$
S_{r1}	1.4167×10^{-15}	$\sec^{-2}$
S_{t0}	-1.2×10^{-8}	$\sec^{-1}$
S_{t1}	7.5×10^{-16}	$\sec^{-2}$
c_1	2×10^{-12}	$(\text{MPa sec})^{-1}$
c_2	2×10^{-12}	$(\text{MPa sec})^{-1}$
p_0	0	MPa
p_1	-2×10^{-6}	MPa/sec
q_0	-1	MPa
q_1	-1.25×10^{-7}	MPa/sec

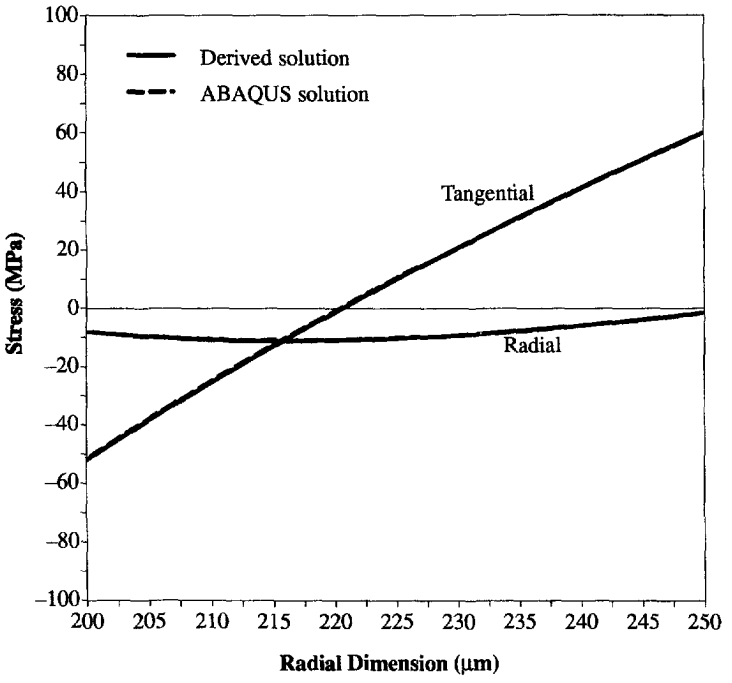

Fig. 4. Comparison of solutions at time 0.4×10^7 sec.

The analytical solution was found to be much easier to implement than the finite element solution. A numerical solution to eqn (29) to determine the function F was readily programmable. With values for F known, the calculations to determine stresses from eqns (26) and (30) involved straightforward algebra. Development of a finite element model was more complicated as it required caution in establishing proper boundary conditions and material property orientations, and in preparing a creep subroutine. Errors committed in this process tended to be subtle, and therefore not always readily detectable. The analytical solution also enjoyed a great advantage in computational time required. Problems that required several minutes of computer processing time to solve using the finite element approach on a mainframe computer required only a fraction of a second using the derived solution.

4. APPLICATION TO PARTICLE MODELING

As stated previously, the solution above can be applied to multilayered particles by imposing continuity of displacements at the interfaces between layers. A full solution for a

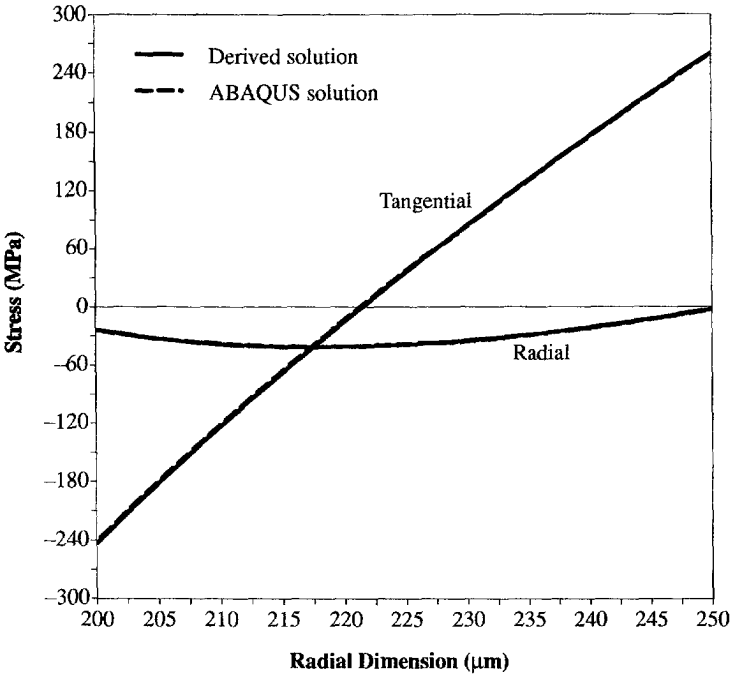

Fig. 5. Comparison of solutions at time 1.2×10^7 sec.

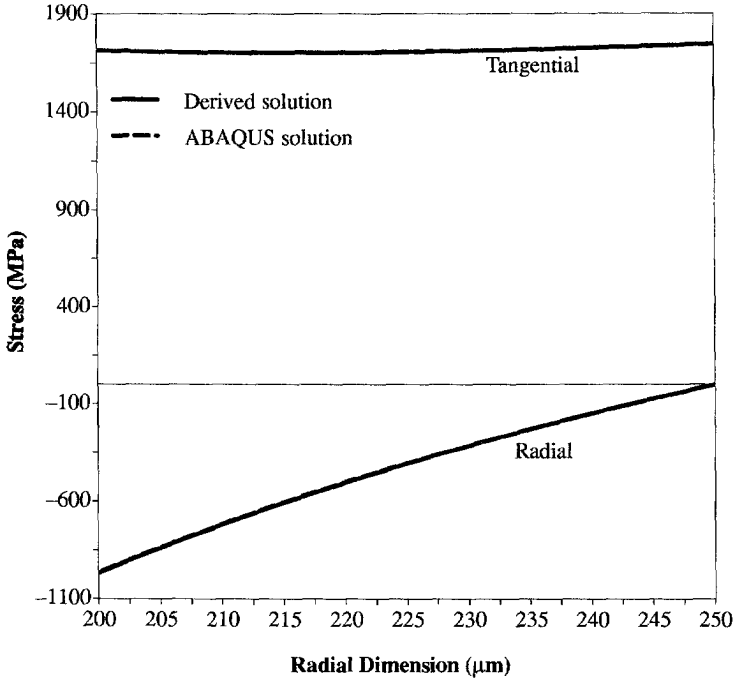

Fig. 6. Comparisons involving displacement equations.

three-layer particle will not be presented herein. A sense for the particle behavior can be gained, though, by considering a two-layer particle consisting of the SiC and OPyC layers. This would correspond to the three-layer particle shown in Fig. 1 without the IPyC layer. The elastic SiC layer is assumed to be considerably more rigid than the OPyC layer, such that the displacement at the interface is set equal to zero. In practice, this is generally a reasonable assumption. A particle failure would occur when the tangential stress in the SiC layer exceeds its tensile fracture strength. Therefore, the stresses of primary interest in this problem are the radial stress at the interface between layers and the tangential stress at the

Table 2. Parameters used for prototypical fuel

Parameter	Value	Units
r_0	252.5	μm
r_1	287.5	μm
r_2	327.5	μm
E_1	3.5×10^4	MPa
E_2	4×10^4	MPa
μ	0.3	
S_{r0}	-3.354×10^{-2}	$(10^{25}\ \text{n/m}^2)^{-1}$
S_{r1}	4.472×10^{-2}	$(10^{25}\ \text{n/m}^2)^{-2}$
S_{r2}	-1.253×10^{-2}	$(10^{25}\ \text{n/m}^2)^{-3}$
S_{r3}	1.343×10^{-3}	$(10^{25}\ \text{n/m}^2)^{-4}$
S_{t0}	-4.147×10^{-2}	$(10^{25}\ \text{n/m}^2)^{-1}$
S_{t1}	2.926×10^{-2}	$(10^{25}\ \text{n/m}^2)^{-2}$
S_{t2}	-9.333×10^{-3}	$(10^{25}\ \text{n/m}^2)^{-3}$
S_{t3}	9.836×10^{-4}	$(10^{25}\ \text{n/m}^2)^{-4}$
c_1	6.222×10^{-4}	$(\text{MPa}\ 10^{25}\ \text{n/m}^2)^{-1}$
c_2	6.222×10^{-4}	$(\text{MPa}\ 10^{25}\ \text{n/m}^2)^{-1}$
p_0	0	MPa
p_1	-6	$\text{MPa}/(10^{25}\ \text{n/m}^2)$
q_0	-6.38	MPa

inner radius of the SiC layer (where it is maximum). The radial stress at the interface shows how the behavior of the OPyC layer affects the SiC layer.

The specific parameters for a prototypical fuel particle are presented in Table 2. The transient creep constants E_2 and c_2 are fictitious since these constants have not yet been determined for prototypical pyrocarbons. The solution was run to a final fast fluence of 4×10^{25} n/m^2. The radii r_0, r_1, and r_2 correspond to the inner radius of the SiC, the outer radius of the SiC, and the outer radius of the OPyC, respectively. The irradiation-induced swelling rate histories were represented with third-order polynomials having coefficients S_{r0}, S_{r1}, etc. The internal pressure was assumed to ramp linearly through the solution from an initial value of zero to a final value of 24 MPa and was applied to the inner radius of the SiC. The external pressure was assumed to be constant and was applied to the outer radius of the OPyC. The radial stress at the interface (r_1) was found by applying eqn (31) at r_1 and setting the displacement equal to zero. The tangential stress at r_0 was found by using eqn (30) without the last term. The pressure q in eqn (30) was the radial stress at the interface.

The solution for the radial stress at the interface is presented in Fig. 7. The solid line shows that the shrinkage in the OPyC layer onto the nonyielding SiC surface caused the compressive (radial) stress at the interface to increase initially. However, the creep in the OPyC layer relaxed this stress until it reached a value of approximately 16 MPa. The dashed line corresponding to the case where there is no transient creep shows that transient creep had some effect on the stress early in the solution but had virtually no effect late in the solution. This may not be representative of true particle behavior since the transient creep constants were not necessarily realistic. Finally, the dashed line corresponding to a case where there is no creep verifies that the stress would in this case continually increase with shrinkage of the OPyC layer.

The solution for the tangential stress in the SiC is presented in Fig. 8. The solid dark line shows that the shrinkage of the OPyC layer onto the SiC caused a compressive tangential stress that initially increased with fluence. When creep in the OPyC relaxed the interface stress, though, the tangential stress reversed and eventually became tensile as the internal pressure increased. Again, the upper dashed line shows that the transient creep in the OPyC had some effect early in the solution, but its effect was recovered later in the solution. The lower dashed line shows that the shrinkage of the OPyC layer overwhelms the internal pressure loading when there is no creep. It can be concluded that the stress relaxation due to creep in the OPyC layer could contribute significantly to particle failures. Similar behavior occurs at elevated temperatures, where stress relaxation due to thermal creep in the OPyC contributes to particle failures.

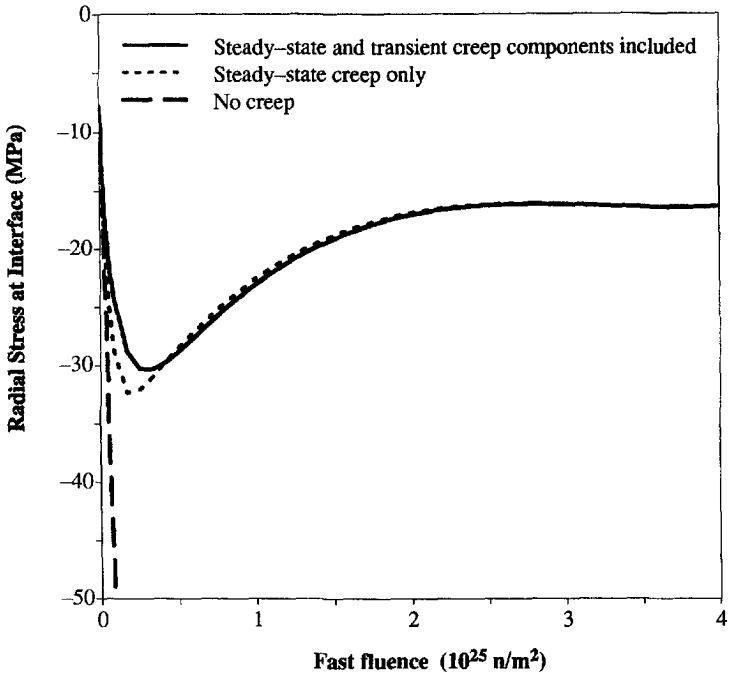

Fig. 7. Radial stress at the inner radius of the pyrocarbon layer.

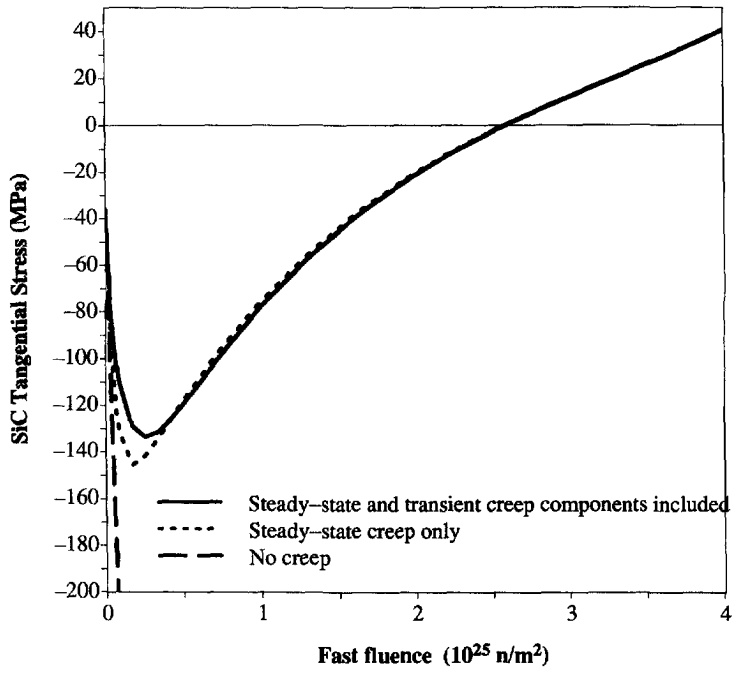

Fig. 8. Tangential stress at the inner radius of the silicon carbide layer.

Some notion as to the stress relaxation time associated with creep can be gained by applying eqn (31) at the interface, momentarily dropping transient creep from consideration. Then, eqn (31) becomes

$$\frac{\mathrm{d}p}{\mathrm{d}t}+\frac{b}{a}p=\frac{1}{a}\left[4r_2^3(\ln r_1-\ln r_2)(S_r-S_t)+\frac{4}{3}(r_2^3-r_1^3)(S_r+2S_t)+bq\right] \tag{51}$$

where

$$a = 2[2r_1^3(k-m)+r_2^3(l+m)]$$

$$b = 3r_2^3 c_1.$$

Because the solution to eqn (51) is

$$p = e^{-\frac{b}{a}t}\left(\int_0^t e^{\frac{b}{a}t'}(\text{RHS})\,dt' + p_0\right) \tag{52}$$

where RHS designates the right hand side of eqn (51), a measure of the "stress relaxation time" (τ) becomes

$$\tau = \frac{a}{b} = \frac{2[2r_1^3(k-m)+r_2^3(l+m)]}{3r_2^3 c_1}. \tag{53}$$

In the case of the prototypical fuel particle, this gives $\tau = 0.0564 \times 10^{25}$ n/m^2.

5. CONCLUSION

The solution presented for stresses and displacements in a spherical pressure vessel considers strains caused by creep and dimensional changes, in addition to instantaneous elastic response. It was developed for modeling of the coated particles in a high temperature gas-cooled reactor. Thus, the creep and dimensional changes considered are either irradiation-induced (reflective of normal operation) or temperature-induced (reflective of accident conditions). The creep behavior in the solution is represented by linear viscoelastic models. This solution is computationally much faster than finite element or finite difference methods. This enables the solution to be used in the Monte Carlo method for determining failure probabilities for large particle populations. The solution has been used here to demonstrate how the stress relaxation due to creep in the pyrocarbon layers of the coated particles can contribute significantly to particle failures.

The analytical approach used for a spherical vessel should be useful in solving for similar loadings on other symmetrical vessel geometries.

REFERENCES

ABAQUS, Version 5.2 (1992). User's Manual, Hibbitt, Karlsson, and Sorensen, Inc., Providence, RI.

Bennett, R. G. (1991). Finite element stress analysis for coated particle fuel modeling under normal operating conditions. *Nucl. Technol.* **96,** 117.

Dobranich, D. and El-Genk M. S. (1991). Thermal stress analyses of the multilayered fuel particles of a particle-bed reactor. *Nucl. Technol.* **94,** 372.

Ferry, J. D. (1980), *Viscoelastic Properties of Polymers*. Third Edition, John Wiley and Sons, Inc.

Kaae, J. L. (1975). Irradiation-induced microstructural changes in isotropic pyrolytic carbons. *J. Nucl. Mater.*, **57,** 82.

Lin, T. H. (1968). *Theory of Inelastic Structures*. John Wiley and Sons, Inc.

Miller, G. K. and Bennett R. G. (1993). Analytical solution for stresses in TRISO-coated particles. *J. Nucl. Mater.* **206,** 35.
Price, R. J. (1977). Properties of silicon carbide for nuclear fuel particle coatings. *Nucl. Technol.*, **35,** 320.
Sokolnikoff, I. S. (1956). *Mathematical Theory of Elasticity*. Second Edition. McGraw–Hill.
Timoshenko, S. and Goodier J. N. (1951). *Theory of Elasticity*. Second Edition. McGraw–Hill.
Tschoegl, N. W. (1989). *The Phenomenological Theory of Linear Viscoelastic Behavior*. Springer-Verlag, Berlin, Heidelberg.